Nonlinear secondary noise sources for passive defect detection using ultrasound sensors

Lynda Chehami, Emmanuel Moulin, Julien de Rosny, Claire Prada, Eric Chatelet, Giovanna Lacerra, Konstantinos Gryllias, Francesco Massi

Journal of Sound and Vibration 386 (2017) 283–294

Nonlinear secondary noise sources for passive defect detection using ultrasound sensors

Lynda Chehami [a,b,*], Emmanuel Moulin [a], Julien de Rosny [b], Claire Prada [b], Eric Chatelet [c], Giovanna Lacerra [c], Konstantinos Gryllias [c,e], Francesco Massi [d]

[a] IEMN UMR CNRS 8520 – University of Valenciennes and Hainaut-Cambresis, F59313 Valenciennes Cedex 09, France
[b] Institut Langevin UMR CNRS 7587, ESPCI ParisTech, F75231 Paris Cedex 05, France
[c] LaMCoS UMR CNRS 5259, INSA University of Lyon, F69621 Lyon Cedex, France
[d] University of Rome 'La Sapienza' – Department of Mechanical and Aerospace Engineering, 00184 Rome, Italy
[e] Faculty of Engineering, Department of Mechanical Engineering, Division PMA, KU Leuven, Celestijnenlaan 300, Box 2420, 3001 Leuven, Belgium

Article info

Keywords:
Friction-induced vibrations Noise correlation
Defect localisation

Abstract

This paper introduces the concept of secondary noise sources for passive defect detection and localization in structures. The proposed solution allows for the exploitation of the principle of Green's function reconstruction from noise correlation, even in the absence of an adequate ambient noise. The main principle is to convert a part of low-frequency modal vibrations into high-frequency noise by exploiting the frictional contact nonlinearities. The device consists of a mass-spring resonator coupled to a flexible beam by a rough frictional interface. The extremity of the beam, attached to the surface of a plate, excites efficiently flexural waves in the plate up to 30 kHz when the primary resonator vibrates around its natural frequency, i.e. a few dozens Hz. A set of such devices is placed at random positions on the plate surface, and low-frequency excitation is provided by a shaker. The generated high-frequency noise is recorded by an array of eight piezoelectric transducers attached to the plate. A differential correlation matrix is constructed by subtracting correlation functions computed from noise signals at each sensor pairs, before and after the introduction of a local heterogeneity mimicking a defect. A simple array processing then allows for the detection and estimation of the defect location from this differential correlation matrix. Beyond the successful proof of concept, influence of experimental parameters, such as the number of secondary sources or the variability of the position of the shaker application point, is also investigated.

1. Introduction

Theoretical and experimental studies have shown that, under the assumption of diffuse noise, the cross-correlation of the recorded fields in two points A and B of a medium gives access to the impulse response between these points as if one receiver acted as an active source [1–7]. The mathematical expression associated to this property is

$$\frac{\mathrm{d}}{\mathrm{d}t}C(A, B, t) \propto \left[G(A, B, t) - G(A, B, -t) \right], \tag{1}$$

where C is the cross-correlation, and G is the medium Green's function.

* Corresponding author at: IEMN UMR CNRS 8520 – University of Valenciennes and Hainaut-Cambresis, F59313 Valenciennes Cedex 09, France.
E-mail address: chehamily@hotmail.fr (L. Chehami).

In ultrasound applications, and particularly in structural health monitoring field, power consumption and complexity of the electronics might represent key issues for the standard methods used in active configurations (pitch-catch). An alternative way could then consist in taking benefit of ambient noise to reveal defects (cracks, holes, …) by passively estimating the Green's functions using the physical principle illustrated by Eq. (1).

The possibility of detecting and localizing defects using ambient noise (friction noise, acoustic noise…) more or less uniformly generated on surface plates has been demonstrated numerically and experimentally in recent works [8,9]. Suitable noise sources for this application should be uncorrelated, with fixed locations and with wideband frequency contents in the ultrasound range. Such source characteristics might not be often available in a natural way. On the other hand, low frequency vibrations sources are common in a number of applications, including transportation, machinery, etc. These sources preferentially excite the first structural modes. Since they are very low frequency, strongly correlated from a point to another and possibly non-stationary, such vibrations cannot be used for the passive defect localization application. To overcome this problem, a prototype of an artificial secondary "passive" acoustic source is proposed. Its role is to transfer part of the energy from the ambient low frequency (LF) vibrations to a secondary high frequency (HF) field by exploiting the frictional contact nonlinearities.

Generally, friction resulting from the sliding contact between two solids, gives rise to diverse forms of waves within solids and frequently leads to undesirable sounds (brake noise, rail-wheel noise…) in the surrounding medium [10–13]. Dry friction-induced vibrations have been the subject of a huge amount of research works, particularly in acoustics [14,15,11,16–21], where the usual objective is to minimize unwanted acoustic emissions. However, recent works [22] have investigated the possibility of using friction nonlinearities as a tool for transferring energy from an acoustic field to another one at different frequencies. In this context, the development of an artificial acoustic secondary source, needed for passive SHM applications, is based on a system constituted by a primary resonator that is connected to a secondary one by a rough sliding interface. The vibration of the main resonator, induced by the ambient low-frequency noise, allows the frictional sliding at the contact interface with the secondary resonator. The dry frictional contact provides then a wideband excitation, generated by nonlinear friction-related effects (roughness, stick-slip, …), which excites the secondary resonator and generates a secondary acoustic field with wide frequency spectrum. The generated secondary field is shown to efficiently excite the flexural waves (A_0 Lamb mode) on an elastic plate in the ultrasound range.

The paper is structured as follows: In Section 2, the passive defect localization method based on the correlation technique, developed in previous works [8,9], is introduced and serves as the reference technique. Then, Section 3 reports the design of the secondary acoustic source and the principle of the energy transferring by dry friction. In Section 4, the HF secondary noise generated by the proposed device is used to detect defects in plate-like structures. In Section 5, the analysis of the effect of a variable position of the LF excitation point on the defect localization images is presented. Finally, some conclusions are presented in Section 6.

2. Passive defect localization

A reverberating plate with a set of transducers fixed on its surface and subject to ambient acoustic noise is considered. It has been shown in a recent work [8] that the differential correlation matrix, that is obtained from the subtraction of the correlation matrices with and without defect, can be expressed as

$$\Delta\mathbf{C}(t) = [\Delta\mathbf{G}(t) - \Delta\mathbf{G}(-t)] \otimes f(t) + \Delta\mathbf{n}(t), \tag{2}$$

where $\Delta\mathbf{G}$ is the part of the Green's function due to the defect and $\Delta\mathbf{n}$ is called the correlation residue (or reconstruction error). This second term corresponds to the part of the differential correlation that is not included in the first term $[\Delta\mathbf{G}(t) - \Delta\mathbf{G}(-t)] \otimes f(t)$. Since this first term can be interpreted as a passive retrieval of information contained in the Green's function, $\Delta\mathbf{n}$ corresponds to a spurious residual that will not contribute to the detection. It strongly depends on the number and the distribution of noise sources (more details about the correlation residue are given in previous works [8,9]). Function $f(t)$ can be considered as a virtual excitation waveform and is given by

$$f(t) = \frac{N_S \tau_a}{2\mathcal{S}\rho h} \int_{-\infty}^{t} R_n(\tau) d\tau, \tag{3}$$

with h the plate thickness, ρ the volume density, $\mathcal{S}$ the plate area, $R_n(\tau)$ the autocorrelation of the noise source and τ_a the characteristic attenuation time constant of the plate.

As shown in previous works [8,9], this differential correlation matrix can be used as the input of a defect localization algorithm, as though it was an actively acquired signal matrix. However, two conditions are necessary for efficient detection: first the noise should have non-negligible components in the useful frequency band (where wavelengths are of the same order of magnitude as the defect size) and second, the correlation residue should be small compared to $\Delta\mathbf{G}(t) \otimes f(t)$.

The second condition means that the noise sources should be both uncorrelated and well distributed over the plate surface or at least, as will be explained later, with unchanged spatial distribution between the acquisitions with and without defect. This can be illustrated through the following considerations. Notations A and B refer to two given spatial distribution configurations of the noise sources used for the acquisition of the correlation matrix without and with defect, respectively. The expression of the reconstruction error can then be written as

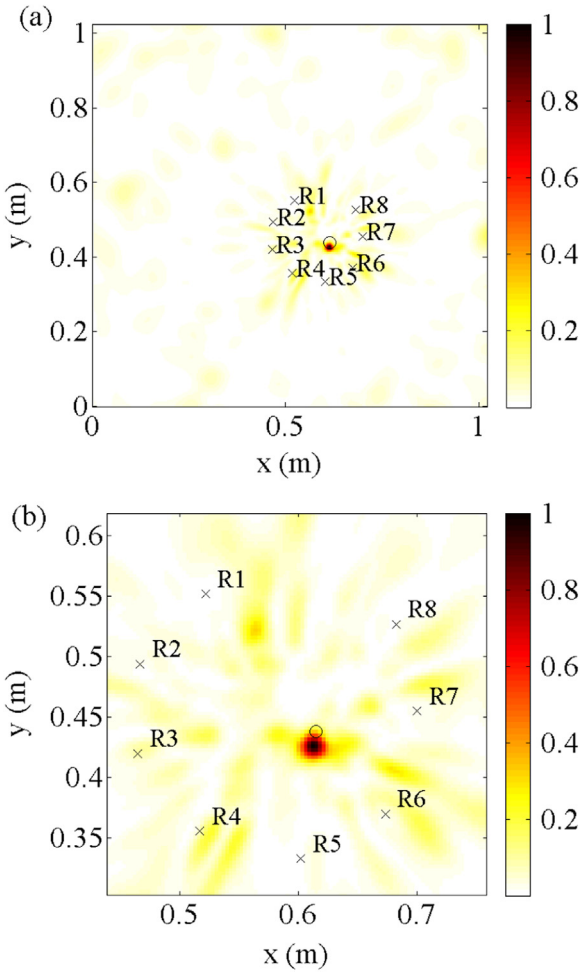

Fig. 1. Defect localization image from loudspeaker-generated noise. (a) Full-field image. (b) Zoom centered on the defect position.

$$\Delta\mathbf{n}(t) = \mathbf{n}_B(t) - \mathbf{n}_A(t) + \delta\mathbf{n}_B(t), \tag{4}$$

where $\mathbf{n}_A$ and $\mathbf{n}_B$ are the correlation residues obtained for the source configurations A and B, respectively, and without the defect. $\delta\mathbf{n}_B$ is the difference of the residues obtained with and without defect, for the noise sources in configuration B.

When configurations A and B correspond to ideally distributed noise sources, $\mathbf{n}_A$ and $\mathbf{n}_B + \delta\mathbf{n}_B$ are very small and $\Delta\mathbf{n}(t)$ is negligible in Eq. (2). Then, $\Delta\mathbf{C}(t)$ can be used for defect detection. An experimental example of passive localization image, obtained when these conditions are fulfilled, is presented in Fig. 1. The plate is 1 m × 1 m and 3-mm thick, made of aluminum. Noise is generated by a loudspeaker fed with electrical white noise and manually swept over the whole plate surface at a distance of about 5 cm to 10 cm from the surface. Before correlations, two operations are performed on the raw signals recorded on the receivers array (R1, …, R8). First, the amplitude of the envelope of time-dependent noise is normalized to compensate the temporal fluctuations. Second, a frequency whitening is performed on the obtained signals between 0.5 kHz and 30 kHz. For experimental repeatability purposes, the considered defect is a pair of cylindrical magnets (diameter 9 mm, height 10 mm) facing each other on the opposite sides of the plate and coupled to the plate with honey. Contrary to an actual material damage, this has the advantage of being removable at will. In Fig. 1, the positions of receivers are indicated by a cross and the defect position by a circle.

The principle of the algorithm used here is based on back-propagating each element of indexes (i,j) of the matrix $\Delta\mathbf{C}$ according to the current pixel position (x,y). The back-propagation function (bpf) of $\Delta\mathbf{C}$ is given by [8]

$$\mathrm{bpf}_{(x,y)}(\omega) = \sum_{i=1,j=1(i\neq j)}^{N_R,N_R} \Delta\mathbf{C}_{ij}(\omega) e^{j\left[d_i(x,y)+d_j(x,y)\right]k(\omega)}, \tag{5}$$

where $d_i(x, y)$ is the distance between the i^{th} receiver and the pixel at position (x,y), $k(\omega)$ is the wave number of the Lamb mode A_0, $\Delta\mathbf{C}_{ij}(\omega)$ is the Fourier transform of $\Delta\mathbf{C}_{ij}(t)$ and N_R is the number of elements in the array (eight in this example). The bpf function leads to a constructive sum and a maximum of the pixel intensity on the defect location [8]. As for pixels

located elsewhere, the obtained intensity is made up of a summation of non-coherent contributions (including correlation residues $\Delta\mathbf{n}$, reverberated wavepackets, grating lobes). It should be noted that since the wavenumber k is neither spatially nor directionally-dependent, the application of Eq. (5) requires the plate area including the sensors and the defect to be homogeneous and isotropic.

As explained above, the reason for the successful defect localization observed on Fig. 1 is essentially the fact that the noise sources are distributed over the whole plate area. Going back to Eq. (4), there appears however another possibility for the correlation residue $\Delta\mathbf{n}$ to be small. Indeed if the source configurations A and B are the same before and after defect, then even if $\mathbf{n}_A(t)$ is non-negligible, the subtraction between correlation matrices cancels this contribution and only $\delta\mathbf{n}_B(t)$ remains in Eq. (4). If the defect is a moderate change in the medium, then $\delta\mathbf{n}_B$ is expected to be small enough to allow the localization of the defect, despite non-perfect reconstruction of the Green's function.

This consideration explains that the passive imaging principle is still successfully applicable with even a moderate number of localized noise sources, as already observed in previous works [8]. This principle will be applied again in Section 4 of this paper, where noise sources of a particular type will be used. Indeed, in order to extend the application range of the correlation technique, a concept of secondary acoustic source that will convert a part of the ambient mechanical vibrations into high-frequency noise components compatible with the defect localization application is proposed. The concept and the preliminary characterization of the proposed devices are presented in the following section. Then, they are used for passive defect detection in the remaining sections.

3. Energy transfer from ambient LF noise to secondary HF field

The main novelty of the proposed approach is the conversion of a part of the low frequency vibratory energy into high frequency components compatible with the application. The nonlinear phenomena associated to the solid frictional contact is shown to be a convenient vector of such conversion.

3.1. Description of the conversion device

The designed device is a mechanical system composed by two resonators connected by a frictional interface. Depending on the application, two different versions of the device have been developed. Fig. 2-(a) shows an advanced design with a compliant system as the main resonator and a beam as secondary resonator. The low frequency vibration of the structure excites the first mode of the compliant system, allowing the relative motion between its contacting surface and the tip of the beam (secondary resonator). The frictional contact provides a large band excitation that excites the higher frequency dynamics of the secondary resonator. The design of this device has been presented in more details in a previous paper [23]. Its compliant structure has the advantage of allowing for the characterisation of the friction-induced acoustic emissions without any disturbance from other parasitic sources of friction.

For the present work, in order to multiply easily the number of the secondary acoustic sources, a simpler design has been used (Fig. 2-b). The primary resonator is a mere spring-mass oscillator, whose natural frequency is tuned to the low frequency

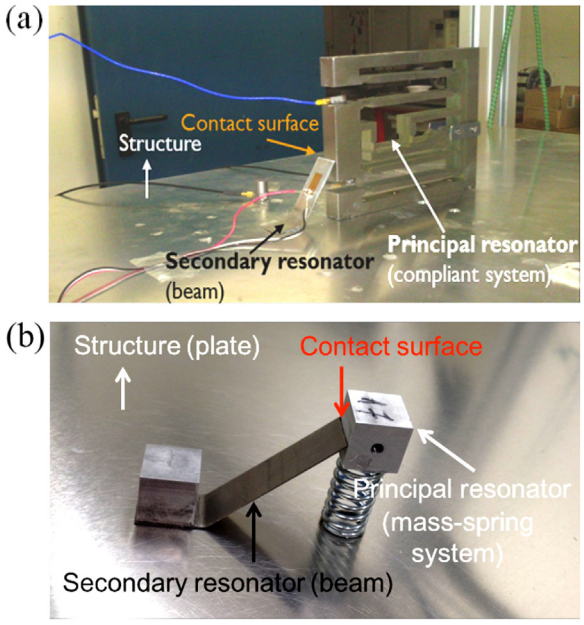

Fig. 2. Secondary acoustic source device: (a) device with principal resonator corresponding to a compliant system; (b) device with principal resonator corresponding to a spring-mass system.

(LF) structural vibrations of the structure (plate). The lateral surface of the mass, oscillating along the vertical direction, interacts by dry frictional contact with the tip of the beam, which is the secondary resonator. This secondary resonator is a flexible beam with one side in frictional contact with the mass of the first resonator and its opposite side rigidly bonded on the structure.

The vibration of the primary resonator, induced by the ambient LF field, allows frictional sliding at the contact surface with the secondary resonator. In such a way a part of the LF vibratory energy is transferred to the secondary resonator by the random excitation at the frictional contact interface. This nonlinear interaction will then excite the modes of the clamped beam over a wide frequency range, depending on the contact characteristics such as roughness, static contact force, relative velocity of the sliding solids, and so on. Finally, part of the vibratory energy of the second resonator will leak into the plate in the form of plate waves, thus constituting a secondary acoustic field in the plate. The characteristics of contact-induced vibrations in the presence of roughness [11,22] allow to expect the presence of frequency components compatible with the application in the secondary field (typically a few kHz to a few dozens kHz).

The working principle of this device can be explained and modeled [22] by considering the three degrees-of-freedom system presented in Fig. 3. m_p, m_s and m_a are lumped masses accounting for the masses of the primary and secondary resonators and of the locally deformed structure. k_p, k_s and k_a are the corresponding lumped stiffnesses. C_p, C_s and C_a are respectively the viscous damping coefficients for the primary and secondary resonators and the local deformation of the structure. Finally, the dry contact friction is modeled by a slider element with tangential constant stiffness k_t (macroslip model associated to a node to node contact element).

Function $y(t)$ is the absolute displacement at the structure surface, $x(t)$ the absolute displacement of the mass m_p from its equilibrium position, and $z(t)$ the relative displacement between the mass m_p and the contact point at the slider interface. When the mass m_p moves at velocity $\dot{x}$, the dynamic response of the primary resonator generates a nonlinear dry friction force (F_{nl}) at the contact surface which can be written as

$$F_{nl}(t) = \begin{cases} k_t(x - y - z) & \text{(sticking condition)}, \\ (1 + \alpha n)\mu N \ \text{sign}(\dot{x} - \dot{y}) & \text{(sliding condition)}, \end{cases} \tag{6}$$

where N is the normal force and $\mu = |F_{nl}|/|N|$ is the average coefficient of friction defined by the Coulomb's law. The wide band dynamic excitation coming from the frictional contact, due mainly to the roughness and ruptures effects, is added as a random disturbance at the contact force during the slipping. This disturbance follows a Gaussian distribution with zero mean value and standard deviation equal to $\alpha|\mu N \text{sign}(\dot{x} - \dot{y})|$. The coefficient α is set in order to reproduce the level of the perturbation due to roughness on the excitation at the contact [22] and $n \sim \mathcal{N}(0, 1)$ is a zero-mean, unit-variance Gaussian random variable.

Thanks to the nonlinearities of friction, generated mainly during the “slipping”, and introduced into the model by the nonlinear contact force, the primary resonator is coupled to the second resonator, which responds with its own resonance, transferring energy to the structure at its frequency.

In this work, the acoustic signals generated by the secondary sources will be measured experimentally using the same piezoelectric transducers as in the loudspeaker-generated noise experiment of Section 2.

3.2. Preliminary experimental characterization

The same plate as in the example presented in Section 2 is considered. Low frequency excitation is provided by a shaker attached at a point of the plate surface indicated by a yellow star in Fig. 4-(a). Twelve nonlinear secondary acoustic source devices (S_1, …, S_{12}) have been glued on the plate, at arbitrary positions indicated by ‘+’.

An experimental characterization of the frequency content of the secondary field generated by the devices is performed. In a first experiment, the relative motion between the primary and secondary resonators at the contact interface has been avoided on all the devices by adding a sheet of paper between the mass surface and the contacting tip of the beam. This action will be referred to as “deactivating” the nonlinear secondary source devices, because it avoids the sliding and thus the wideband excitation coming from the frictional contact. Then, the shaker is excited with a white noise in the frequency band [70, 150] Hz. The average power spectral density of the signals recorded on the transducers is plotted on Fig. 5 (black curve)

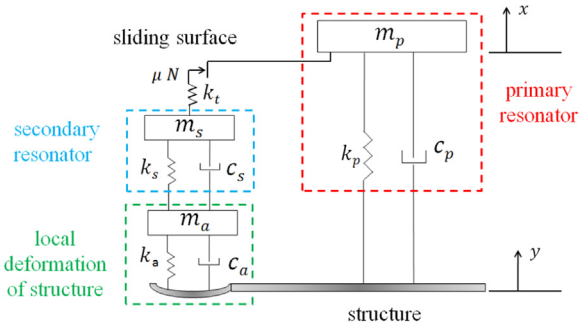

Fig. 3. Simplified 3 degrees-of-freedom model for simulating the energy transfer by frictional contact.

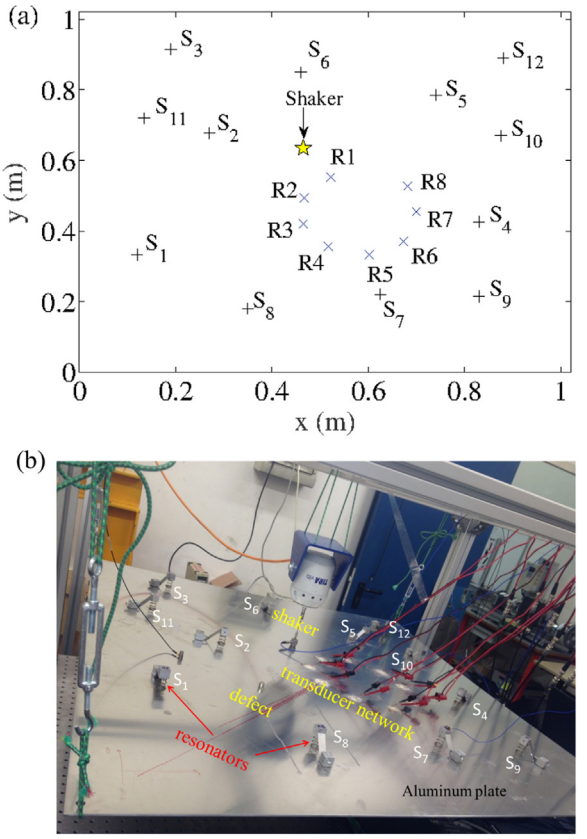

Fig. 4. Experimental setup. (a) Schematic of the positions. (b) Overall set-up.

in logarithmic scale, as a function of frequency. As expected, only the low frequency components excited by the shaker are significant.

The same measurement is performed when reactivating the twelve resonators (blue dashed curve), i. e. when allowing the sliding at the contact by removing the paper. Significant acoustic power appears now in the frequency band [5, 30] kHz, approximately five orders of magnitude higher than the noise level shown by the black curve. These results essentially validate the LF to HF conversion principle. However, similar measurements performed with each single resonator activated at a time (thin colored curves) show a great dispersion in their HF generation behaviors. This point will be further commented in Section 5.

The transducer network (indicated by "x" on Fig. 4-a) used for the localization of defects can also be used for the characterization of these acoustic sources. This requires only a slight modification of the array processing algorithm: the sum of distances in Eq. (5) is replaced by the difference $[d_i(x, y) - d_j(x, y)]$. The rest of the post-processing is exactly the same as in the case of defect localization [8]. This makes the corresponding algorithm similar to beamforming, with wave

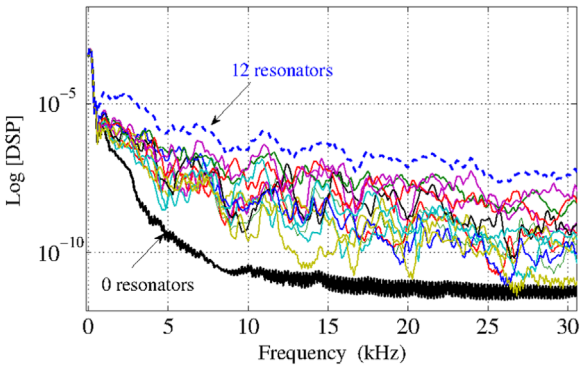

Fig. 5. Averaged power spectral density (PSD) of recorded noise with: all resonators deactivated (black line), all resonators activated (blue dashed curve) and each resonator activated separately (other curves). (For interpretation of the references to color in this figure legend, the reader is referred to the web version of this article.)

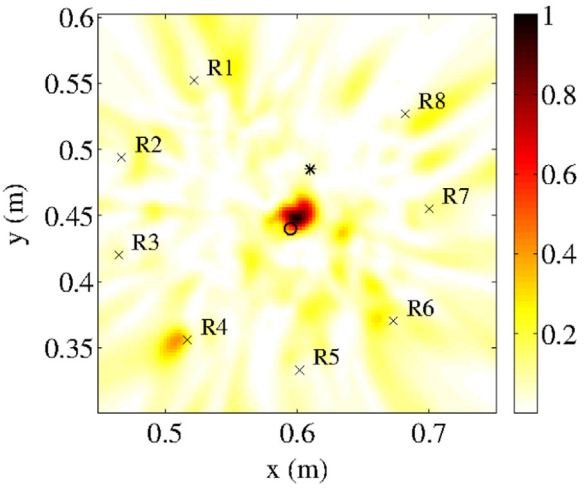

Fig. 6. Beamforming of the noise generated by a single resonator in the frequency range [1, 40] kHz. The position of the secondary resonator (fixing point of flexible beam on the plate) is indicated by a circle and the first resonator (end of the spring fixed on the plate) by a star.

dispersion taken into account. A nonlinear secondary source has been temporarily placed at the middle of the transducer network, which is the best place from the point of view of ratio between focal distance and network aperture. The obtained beamforming image is shown in Fig. 6. The recorded noise is filtered in the frequency-band [1, 40] kHz, prior to cross-correlation. The real positions of the connections of the primary (spring) and secondary (beam) resonators with the plate are also indicated.

As expected, the high frequency content is produced and transfered to the plate by the secondary resonator. This preliminary study and the obtained results let expect a sufficient level of noise in the useful frequency band for defect detection.

4. Application to defect detection and localization

In this section, the applicability of the HF secondary noise for the defect localization technique based on passive noise correlation is verified.

4.1. Validation of the principle

A first defect localization test has been performed on the same plate as in the previous sections, with all the secondary sources deactivated. Only the shaker emitted a white noise in the frequency band [70, 150] Hz. The localization image result is displayed on Fig. 7.

As expected, the defect cannot be detected. Only noise-related spurious lobes are visible.

In a second experiment, all the secondary sources S_1 to S_{12} have been reactivated, by allowing the frictional sliding at their contacting interfaces. The corresponding localization images are plotted on Fig. 8 for two defect positions.

In these cases, the defects are efficiently localized and detected. The nonlinear resonators thus play their role of secondary sources for ultrasound imaging. The quality of Fig. 8-(a), where the defect is inside the network, is better than Fig. 8-(b), where the defect is outside. This effect, also observed with classical HF noise sources [9], is directly related to the effective aperture of the sensors array versus the defect position.

In the next section, the influence of the number of secondary sources on the localization images will be investigated.

4.2. Influence of the number of secondary noise sources

Experimental tests have been performed with 8, 4 and 2 secondary sources, respectively, when the defect is located inside the transducer array. The corresponding images are displayed in Fig. 9 for a defect located at the same position, indicated by the black circle. The positions of the secondary sources are indicated by '+' in each case.

In this case, where it is in a favourable position for being detected, the defect remains localized with as few as four secondary sources. These results confirm the fact, already observed in previous works [9], that a perfect reconstruction of the Green's functions is not absolutely necessary to the defect localization application. Therefore, even a relatively low number of noise sources might be enough, provided they emit from the same locations before and after the defect.

However, the average level of spurious lobes obviously grows as the number of secondary nonlinear sources decreases. This is quantified in Fig. 10, where the spurious lobe average levels, excluding the location of the maximum of the defect lobe (0 in dB scale), are plotted. This phenomenon is caused by the fact that the cancellation of the unwanted contribution

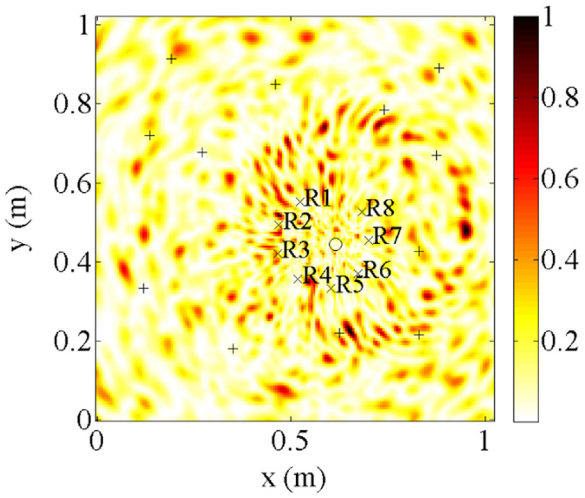

Fig. 7. Defect localization image obtained with all secondary sources (S_1 to S_{12} indicated by '+') deactivated. The defect position is indicated by a black circle.

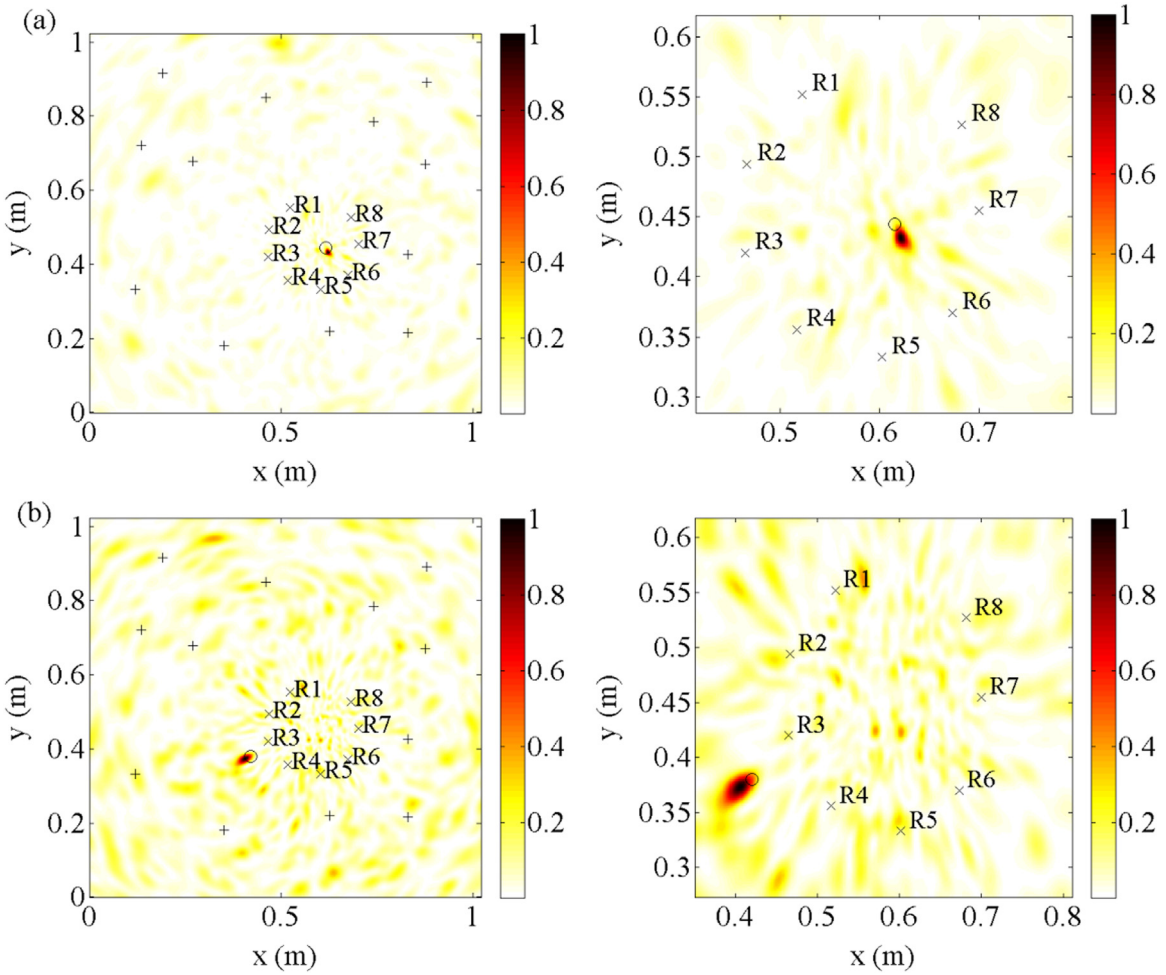

Fig. 8. Defect localization images obtained with all secondary sources (S_1 to S_{12} indicated by '+') activated, for two different scatterer positions (top and bottom subfigures, respectively). (left) Full-field images. (right) Zooms on the transducer array. Defect positions are indicated by black circles.

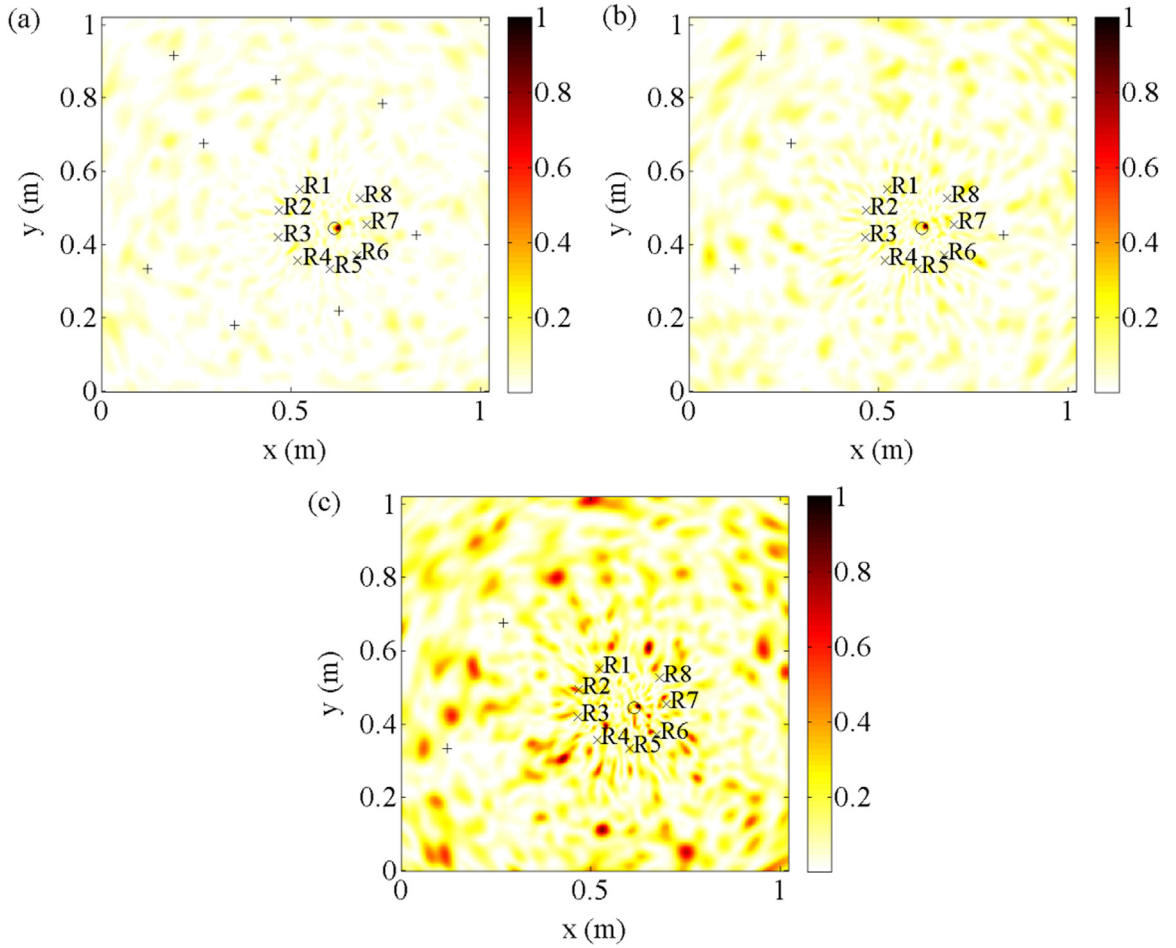

Fig. 9. Defect localization images obtained with different numbers of activated secondary sources: (a) 8 sources, (b) 4 sources and (c) 2 sources. The defect position is indicated by a black circle.

$\delta \mathbf{n}_B$ is less efficient when fewer sources are involved, thus degrading the localization image.

The slight increase of the spurious lobe level for 10 and 12 sources can be explained by the variability of the HF emission levels of the devices, as observed in Fig. 5. Indeed, strong secondary sources may blind other weaker ones and therefore decrease the effective spatial diversity of the noise emission.

5. Role of spatial fixedness of the primary LF source

In this section, the effect of a variable position of the low frequency excitation point is studied. To this aim, two additional

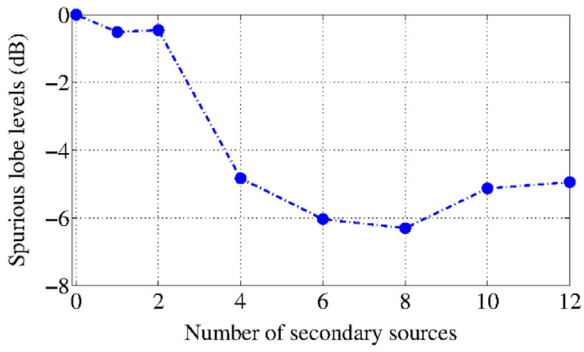

Fig. 10. Spurious lobe average levels excluding the location of the focal spot (a half-wavelength around 0 dB).

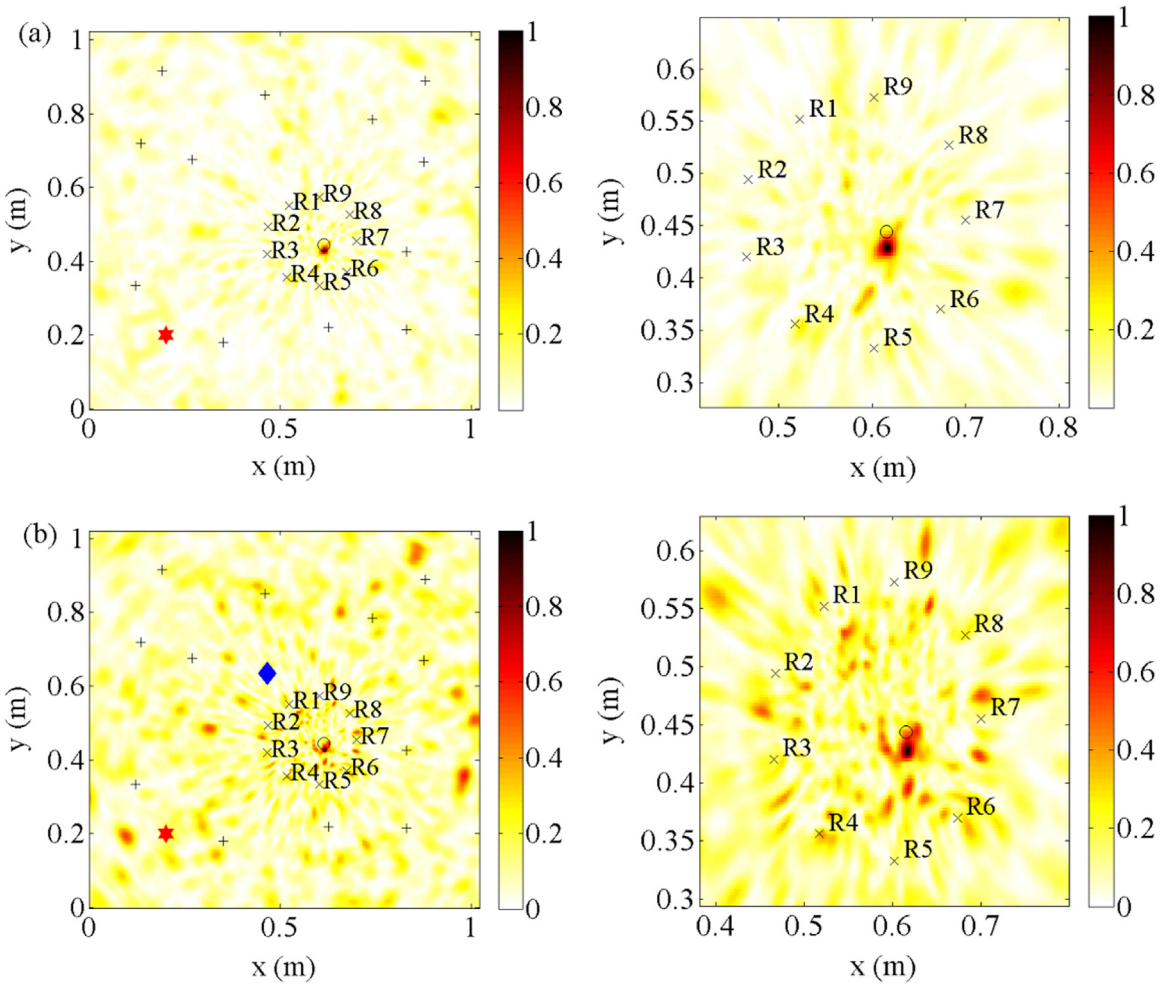

Fig. 11. Defect localization images obtained with all secondary sources activated (S_1 to S_{12} indicated by '+'). (a) The position of the shaker is fixed at position (0.2,0.2) m for both the acquisitions w/o defect (indicated by a red star). (b) The shaker is moved at position (0.465,0.635) m for the reference state (indicated by a lozenge). The defect position is indicated by a black circle. (right) zoom centered on the defect position.

experiments are performed with the same plate as in the previous experiments. First, the application point of the shaker (indicated by a red star on the images) is fixed at position (0.2,0.2) m for both the acquisitions with and without defect. The corresponding localization image, shown in Fig. 11-(a), appears similar to the one in Fig. 8-(a). Then, in the second experiment, the reference acquisition (without defect) and the acquisition with the defect are performed with two different positions of the shaker: (0.465,0.635) m and (0.2,0.2) m, respectively. Though a lobe is obtained on the defect position, the image obtained for this case (Fig. 11-b) is clearly of lower quality.

This result can be interpreted as a sensitivity of the secondary HF emission by the nonlinear sources to the LF excitation point. This sensitivity is directly related to the modal amplitudes and modal shapes of the structural modes excited by the shaker. Indeed, depending on the modal shapes, the relative excitation levels of the primary resonators (mass-spring systems) of the sources will be affected by their positions on the plate. For a given shaker excitation point, a given set of modal amplitudes will thus produce different HF emission levels of the secondary sources, which will correspond to a certain spatial "pattern" of the HF noise field (as already observed in Fig. 5).

When the shaker excitation point is moved, changes of the modal amplitudes will produce a different pattern of the HF field, and the spurious term $\mathbf{n}_B(t) - \mathbf{n}_A(t)$ of Eq. (4) might significantly degrades the image. To confirm this interpretation, an experimental characterization of the spatial radiation distribution is proposed by means of beamforming image computations, similar to Fig. 6. First, the beamforming algorithm is applied on the noise correlation matrix obtained without defect, when the shaker position is (0.2, 0.2) m (see Fig. 12-a). Since the sources are located outside the sensor set (contrary to the single source characterization in Fig. 6), only the angular directions of the HF energy radiation are efficiently retrieved. But this is sufficient for the present purpose. It appears that all secondary sources (indicated by small crosses +) have not exactly the same HF emission levels. Still, the angular energy distribution is relatively homogeneous and is obviously sufficient to perform the defect localization (as demonstrated in Fig. 11-a). Then the beamforming image is computed with the

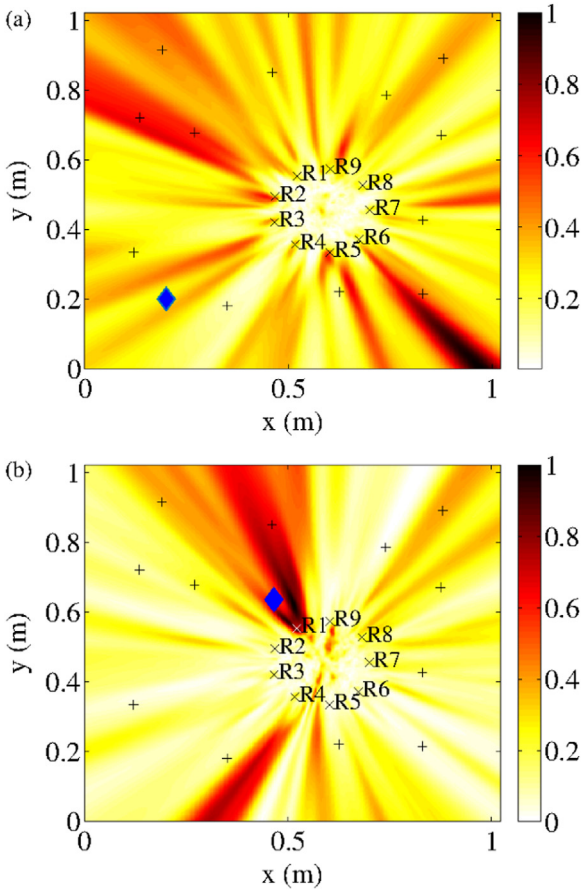

Fig. 12. Beamforming of the noise generated by all 12 resonators in the frequency range [1, 40] kHz. The shaker excitation is applied at position (a) (0.2,0.2) m and (b) (0.465,0.635) m, respectively. The position of the shaker is indicated by a lozenge and the sources by '+'.

shaker at position (0.465, 0.635) m (Fig. 12-b). Clearly the angular energy distribution corresponds to a significantly different pattern. This confirms that two different shaker positions may result in different sets of secondary emission levels.

Possible solutions to mitigate this effect will be investigated in future works. This will require a better understanding and reproducibility of the secondary sources behavior. In particular, imposing a proper compromise between resonances and bandwidth of the primary resonator could help to make the high-frequency emission level less sensitive to the positions.

6. Conclusion

A novel concept of energy transferring from ambient low-frequency (LF) vibrations towards a secondary high-frequency (HF) noise field by exploiting the dry contact frictional nonlinearities has been proposed in this paper. The proposed device is a mechanical system composed by a primary resonator, which is tuned to the LF structural vibrations of the plate, and a secondary resonator (flexible beam), which allows the transferring of HF vibrations. The two resonators are put in frictional contact with each other. The vibration of the primary resonator, induced by the ambient LF field, allows frictional sliding at the contact surface with the secondary resonator. In this way HF friction-induced acoustic emission (due to wide band excitation at the contact) is produced and transmitted to the plate through the secondary resonator.

The acoustic field on the structure has been measured both with and without activation of the frictional devices. The HF noise generated by the devices has appeared to have non-negligible components in the useful frequency range where wavelengths are of the same order of magnitude as the defect size.

These devices have been used as secondary noise sources for passive defect detection and localization based on noise correlation. Satisfying results have been obtained even with a small number of secondary sources. It is shown in particular that even though the secondary sources have not all the same emission levels, the HF energy distribution allows to perform defect localization, provided the LF excitation source is not moved between measurements with and without the defect. Indeed, it has been shown that the variability of the secondary HF emission characteristics, in cases where the LF excitation source position is moved, is not negligible and has the effect of degrading significantly the defect localization images.

Possible solutions to mitigate this effect will be investigated in future works. It is expected that better understanding and optimization of the resonance features of the nonlinear devices will lead to significant improvements.

Acknowledgement

This work has been supported by the French National Research Agency (ANR): Grant ANR2011 BS0903901 (PASNI Project), and by LABEX WIFI (Laboratory of Excellence within the French Program "Investments for the Future") under reference ANR-10-IDEX-0001-02 PSL.

References

[1] O. Lobkis, R. Weaver, On the emergence of the Green's function in the correlations of a diffuse field, *Journal of the Acoustical Society of America* 110 (2001) 3011–3017.
[2] E. Larose, P. Roux, M. Campillo, Reconstruction of Rayleigh-Lamb dispersion spectrum based on noise obtained from an air-jet forcing, *Journal of the Acoustical Society of America* 122 (2007) 3437–3444.
[3] K. Sabra, P. Roux, W. Kuperman, Emergence rate of the time-domain Green's function from the ambient noise cross-correlation function, *Journal of the Acoustical Society of America* 118 (2005) 3524–3531.
[4] K. Sabra, E. Winkel, D. Bourgoyne, B. Elbing, S. Ceccio, M. Perlin, D. Dowling, Using cross-correlations of turbulent flow-induced ambient vibrations to estimate the structural impulse response. Application to structural health monitoring, *Journal of the Acoustical Society of America* 121 (2007) 1987–2005.
[5] E. Moulin, N.A. Leyla, J. Assaad, S. Grondel, Applicability of acoustic noise correlation for structural health monitoring in nondiffuse field conditions, *Applied Physics Letters* 95 (2009) 094104–0941043.
[6] M. Davy, J. de Rosny, M. Fink, Green's function retrieval and passive imaging from correlations of wideband thermal radiations, *Physical Review Letters* 110 (2013) 203901.
[7] T. Nowakowski, L. Daudet, J. de Rosny, Localization of acoustic sensors from passive Green's function estimation, *Journal of the Acoustical Society of America* 138 (2014) 3010–3018.
[8] L. Chehami, E. Moulin, J. de Rosny, C. Prada, O.B. Matar, F. Benmeddour, J. Assaad, Detection and localization of a defect in a reverberant plate using acoustic field correlation, *Journal of Applied Physics* 115 (2014) 104901–1049017.
[9] L. Chehami, J. de Rosny, C. Prada, E. Moulin, J. Assaad, Experimental study of passive defect localization in plates using ambient noise, *IEEE Transactions on Ultrasonics, Ferroelectrics, and Frequency Control* 62 (2015) 1544–1553.
[10] C. Menq, P. Chidamparam, J. Griffin, Friction damping of two-dimensional motion and its application in vibration control, *Journal of Sound and Vibration* 144 (2008) 427–447.
[11] A. Akay, Acoustics of friction, *Journal of the Acoustical Society of America* 111 (2002) 1525–1548.
[12] K. Popp, L. Panning, W. Sextro, Vibration damping by friction forces theory and applications theory and applications, *Journal of Sound and Vibration* 9 (2003) 419–448.
[13] E. Chatelet, G. Michon, L. Manin, G. Jacquet, Stick/slip phenomena in dynamics choice of contact model. Numerical predictions and experiments, *Mechanism and Machine Theory* 43 (2008) 1211–1224.
[14] J. Swayze, A. Akay, Effects of system dynamics on friction-induced oscillations, *Journal of Sound and Vibration* 173 (2007) 599–610.
[15] B. Feeny, A. Guran, N. Hinrichs, K. Popp, A historical review on dry friction and stick-slip phenomena, *Applied Mechanics Reviews* 51 (1998) 321–341.
[16] A. Carcaterra, A. Akay, Theoretical foundations of apparent damping phenomena and nearly-irreversible energy exchange in linear conservative systems, *Journal of the Acoustical Society of America* 121 (2007) 1971–1982.
[17] M.N.A. Emira, Friction-induced oscillations of a slider parametric study of some system parameters, *Journal of Sound and Vibration* 300 (2007) 916–931.
[18] Q. Ding, Y. Chen, Analyzing resonant response of a system with dry friction damper using an analytical method, *Journal of Vibration and Control* 14 (2008) 1111–1123.
[19] M. Bartolomeo, F. Massi, L. Baillet, A. Fregolent, Y. Berthier, A. Culla, Wave and rupture propagation at frictional bimaterial sliding interfaces from local to global dynamics, from stick-slip to continuous sliding, *Tribology International* 52 (2012) 117–131.
[20] D. Tonazzi, F. Massi, A. Culla, L. Baillet, A. Fregolent, Y. Berthier, Instability scenarios between elastic media under frictional contact, *Mechanical Systems and Signal Processing* 40 (2013) 754–766.
[21] M. Bartolomeo, A. Meziane, F. Massi, L. Baillet, A. Fregolent, Dynamic rupture at a frictional interface between dissimilar materials with asperities, *Tribology International* 43 (2010) 1620–1630.
[22] K. Gryllias, E. Chatelet, F. Massi, E. In: Moulin, Energy transfer between aacoustic fields by dry frictional contacts for SHM: a lumped numerical analysis, in: Proceedings of the Sixth International Conference on Noise and Vibration Engineering, KU Leuven, September 2014, pp. 1–15.
[23] G. Lacerra, F. Massi, E. Chatelet, K. In: Gryllias, Design of a mechanical system for energy transfer between acoustic fields by frictional contact nonlinearity, in: Proceedings of the Seventeenth International Symposium on Dynamic Problems of Mechanics, NATAL, February 2015, pp. 1–10.